International Journal of Multiphase Flow 36 (2010) 109–118

Contents lists available at ScienceDirect

International Journal of Multiphase Flow

journal homepage: www.elsevier.com/locate/ijmulflow

Review

A review of multiscale CFD for gas–solid CFB modeling

Wei Wang *, Bona Lu, Nan Zhang, Zhansheng Shi, Jinghai Li *

State Key Laboratory of Multiphase Complex Systems, Institute of Process Engineering, Chinese Academy of Sciences, Beijing 100190, China
Graduate University of Chinese Academy of Sciences, Beijing 100049, China

ARTICLE INFO

Article history:
Received 11 October 2008
Received in revised form 12 January 2009
Accepted 25 January 2009
Available online 12 February 2009

Keywords:
Meso-scale
Multiscale
CFD
Simulation
Fluidized bed
Structure
Mass transfer

ABSTRACT

Meso-scale structure is of critical importance to circulating fluidized bed (CFB) applications. Computational fluid dynamics (CFD) with consideration of meso-scale structures can help understand the structure-oriented coupling between flow, heat/mass transfer and reactions. This article is to review our recent progress on the so-called multiscale CFD (MSCFD), which characterizes the sub-grid meso-scale structure with stability criteria in addition to conservation equations. It is found that the mesh-independent solution of fine-grid two-fluid model (TFM) without sub-grid structures is inexact, in the sense that it overestimates the drag coefficient and fails to capture the characteristic S-shaped axial profile of voidage in a CFB riser. By comparison, MSCFD approach in terms of EMMS/matrix seems to reach a mesh-independent solution of the sub-grid structure, and succeeds in predicting the axial profile and flow regime transitions. Further application of MSCFD finds that neglect of geometric factors is one of the major reasons that cause disputes in understanding the flow regime transitions in a CFB. The operating diagram should, accordingly, include geometric factors besides commonly believed operating parameters for the intrinsic flow regime diagram. Recent extension of MSCFD to mass transfer finds that Reynolds number is insufficient for correlating the overall Sherwood number in a CFB. This is believed the main reason why the conventional correlations of Sherwood number scatter by several orders of magnitude. Certain jump change of state of motion around Reynolds number of 50–100 can be expected to clarify the abrupt decay of Sherwood number in both classical- and circulating-fluidized beds. Finally, we expect that the real-size, 3-D, full-loop, time-dependent multiscale simulation of CFB is an emerging paradigm that will realize virtual experiment of CFBs.

1. Unclear multiscale structure: obstacle to CFB applications

Compared to classical fluidized beds, circulating fluidized bed (CFB) operates at high gas velocity with solids circulation, which benefits gas–solid contact, bed-to-wall heat transfer, catalyst regeneration, and reaction selectivity. Therefore, it finds wide applications in processes such as aluminum hydroxide calcination, fluid catalytic cracking (FCC), coal combustion (Reh, 1996) and methanol-to-olefin (MTO) (Soundararajan et al., 2001). The whole loop of CFB consists of the riser, downcomer, and in between, cyclone and valve/siphon. Most of researches are focused on the riser section where reactions mainly occur, whose behavior is, however, connected with the other sections of the loop.

CFB flow structure varies with the operating conditions and physical properties. The gas and particles in a CFB are heterogeneously dispersed, resulting in various forms of structures over a wide range of scales as to time and space. If we define the micro-scale as the scale with respect to the smallest space being observed, e.g. one single particle in experiment or one local volume in computation, and define the macro-scale as that with respect to the cross-section averaging under the constraint of boundaries, then, the wide span of scales between the micro- and the macro-scales can be named the meso-scale, which bears the most diverse nature of all structures with rich information. Accordingly, the meso-scale structure is the most important part to understand the flow behavior, and hence, in what follows we will not distinguish the difference between "structure" and "meso-scale structure".

In addition to the operating conditions and physical properties, geometric factors also affect the flow structures, thus complicating the overall performance of CFBs. For example, tube diameter concerns whether the slugging can occur (Yang, 2004); a short riser may be affected significantly by the inlet/outlet effects, showing different profiles from those in a higher riser under the same operating conditions; different connections between the downcomer and the riser may cause different profiles of voidage (Li, 1994).

A flow regime is characterized by its distinctive flow structures. In the literature, between the classical fluidization and pneumatic transport, flow regimes cited may include fast fluidization, dense suspension upflow, dilute upflow and even turbulent fluidization (Kwauk, 1994; Grace et al., 1999; Gidaspow et al., 2004; Breault,

* Corresponding authors. Fax: +86 10 62558065.
E-mail addresses: wangwei@home.ipe.ac.cn (W. Wang), jhli@home.ipe.ac.cn (J. Li).

0301-9322/$ - see front matter © 2009 Elsevier Ltd. All rights reserved.
doi:10.1016/j.ijmultiphaseflow.2009.01.008

2006). However, owing to limited understanding on relevant flow structures, disputes remain on the definitions of different flow regimes and their transitions, in which the choking is a typical example, as recorded in the review by Bi et al. (1993) and Yang (2004).

Structures have strong impact on the interphase momentum transfer and mass transfer, in terms of drag force and mass transfer rate, respectively. The drag force may differ greatly for different structures (Li and Kwauk, 2001; Agrawal et al., 2001; Sundaresan, 2006). Accordingly, the simulation using the conventional drag force coefficient based on homogeneous suspensions may overestimate the solids flux by several orders of magnitude and result in wrong prediction of flow regimes (Yang et al., 2003). Similar situation exists for the mass transfer but receives less concern. One reason is the expectation that the heat/mass transfer rate is high in a CFB and therefore of minor effects to the overall reaction rate. For example, the reaction coefficient k_r of ozone decomposition over FCC particles was reported of the order of magnitude of $10\ s^{-1}$, while that of the overall mass transfer coefficient $k_p\alpha_p$ was $10^5\ s^{-1}$ (Ouyang et al., 1995; Dong et al., 2008a). That means, the overall performance is controlled by reaction rate and the mass transfer is negligible (Damköhler number $Da = k_r/k_p\alpha_p \ll 1$) in the case that the flow is regarded homogeneous. However, heterogeneous structure can result in significant decrease of mass transfer rate, making $Da \sim 1$. As reported in Breault (2006), the mass transfer coefficient in a CFB may differ by 7 orders of magnitude. Given this situation, the conventional approach for mass transfer by treating particles as if they were uniformly suspended by the upward flowing gas greatly simplifies the actual phenomena and complications owing to multiscale structures (Chen, 2003).

Although the structure is important, it is difficult to elucidate structural effects only through experiments. On one hand, different researchers may use quite different geometric designs, operating modes and conditions, which are hard to unify; on the other hand, it is rather difficult, if not impossible, to manipulate in experiment the variation of structures that is dynamic in nature. By comparison, computational fluid dynamics (CFD) allows easy adjustment in these aspects, and thus, it is easy to reach common knowledge on the structural effects. However, current efforts in CFD simulation of CFBs have introduced too much simplification and paid inadequate attention to the multiscale structure. For example, homogeneous assumption was widely adopted in both hydrodynamic, mass transfer and reaction models; three-dimensional (3-D) loop geometries were often simplified with two-dimensional (2-D) rectangular channels (Neri and Gidaspow, 2000; Yang et al., 2004). In view of the importance of structures, these simplified treatments may miss the real mechanisms underlying the complex states of motion. The model taking into account structures should be encouraged, while the kernel relies on whether it correctly characterizes the structure.

2. Meso-scale structure: challenge to CFD simulation

To resolve the meso-scale structure, various CFD approaches have drawn a lot of attention in recent decades. Of these approaches, the time-dependent two-fluid model (TFM) using kinetic theory for granular flow (KTGF), which was pioneered by Gidaspow group (Ding and Gidaspow, 1990; Gidaspow, 1994; Gidaspow et al., 2004), has been widely recognized as a paradigm and the standard for comparison. If we recognized the validity of TFM as a starting point for two-phase flow modeling and assumed homogeneity within each grid, then, in principle, we could finally obtain mesh-independent, real solution of TFM through refining grid, and accordingly, expect to simulate a CFB without losing meso-scale details in the case that the computing capacity was sufficiently high. Such an approach can be termed "fine-grid" simulation. Its demand on the computing capacity is rather high for industrial scale simulation.

Another approach is the so-called "coarse-grid" simulation with apposite sub-grid models, over which two branches can be further classified according to the choice of sub-grid models — one is termed the "correlative" (Li and Kwauk, 2003), it obtains the sub-grid model through performing finer-scale simulation and then statistical averaging. Examples for that may be referred to Agrawal et al. (2001) and Igci et al. (2008), where the effective drag coefficients for coarse-grid simulation were derived from the fine-grid simulation results over periodic domains. The other branch is termed the "variational", it correlates movements between the fine- and coarse-grids (or scales) by invoking a variational stability condition, which is exemplified by the energy minimization multiscale (EMMS) model (Li and Kwauk, 1994) and its extensions, e.g. EMMS/matrix for flow modeling (Wang and Li, 2007) and EMMS/mass for reaction modeling (Dong et al., 2008a).

This article is to review our models on the so-called multiscale CFD (MSCFD). It begins with a brief introduction of EMMS model and its extension, EMMS/matrix, followed by investigation of the effect of grid size and then applications in picturing flow regime transitions and operating diagram for industrial practices. Recent progress extending MSCFD to the domains of mass transfer and reactions is also reviewed. The emerging paradigm to realize the virtual experiment through full-loop simulations of CFB is outlined in brief in the last section. This review aims to address certain critical issues concerning meso-scale structures. These issues refer to, for example, whether the sufficiently fine grid exists for TFM without sub-grid heterogeneity? Whether fine-grid TFM can be used to simulate a real CFB unit with satisfying precision? Which kind of sub-grid models can be expected to reach the mesh-independent solution of the effect of structures? How geometric restrictions affect the flow regime transition in a CFB? How heat/mass transfer is related to the meso-scale structure? Finally, this review will end with concluding remarks and certain viewpoints for prospects.

3. Structure-oriented multiscale CFD

EMMS model characterizes the multiscale structure in riser flows with a bi-scale resolution (Li and Kwauk, 1994), i.e. the cluster scale in terms of particle-rich dense phase (marked by the subscript "*c*") and the dispersed particle scale in terms of fluid-rich dilute phase (marked by the subscript "*f*"). Instead of seeking constraint laws purely from dynamics, Li and Kwauk argued that certain stability condition should be obeyed to sustain the dissipative structure. A variational criterion expressed as $N_{st} \rightarrow \min$ was hence proposed, which suggests "compromise", or in other words, mutual optimization, between gas dominance ($W_{st} \rightarrow \min$) and particle dominance ($\varepsilon \rightarrow \min$). Here, N_{st} denotes mass-specific energy consumption for suspending and transporting particles (W/kg), W_{st} denotes volume-specific energy consumption for suspending and transporting particles (W/m^3), ε denotes voidage. It is the "compromise" that results in the heterogeneous and dissipative structure, either dominance only leading to even distribution. Later exploration on the underlying physics verified this critical presumption through a pseudo-particle method simulation (Zhang et al., 2005). Thus, the total variable set, including the particle velocity (U_{sk}), gas velocity (U_{gk}) and voidage (ε_k) in each phase "*k*" (*k* refers to *c* or *f*), together with the volume fraction of the dense phase (f) and the cluster diameter (d_c), was closed by a set of conservation equations obeyed by each phase and the objective optimization criterion specific to fluidized beds.

EMMS model was proposed for the time–mean behavior under force balance. To couple with CFD, EMMS was further extended to the sub-grid level by taking into account the inertial terms in each phases (a_c, a_f, a_i) and then, used to calculate the drag coefficient

that is critical to two-phase flow in a CFB. This extended model names after EMMS/matrix, which features a two-step scheme (Wang and Li, 2007). The first step is to determine the cluster parameters in terms of the cluster diameter and cluster voidage (d_c and ε_c). The current version of EMMS/matrix adopts the original definitions in EMMS, such that d_c and ε_c are subject to the criterion, $N_{st} \rightarrow \min$, under the given conditions of superficial gas velocity U_g and solid flux G_s. Obviously, alternative models or correlations of d_c and ε_c are acceptable under the framework of this two-step scheme. The remaining variables, i.e. (U_{gc}, U_{sc}, f) for the dense phase and $(U_{gf}, U_{sf}, \varepsilon_f)$ for the dilute phase as well as the inertial terms associated to each phases, are resolved in the second step by deterministic solution of the set of conservation equations. The solution of the second step can be simplified according to the Galilean relativity by organizing the conservation equations as functions of slip velocities (Wang et al., 2008b; Lu et al., submitted for publication). However, the same values of slip velocity and voidage within a grid do not infer the same drag coefficient, as the first step indicates that ε_c and d_c depend additionally on the global conditions of U_g and G_s.

Compared to TFM, EMMS/matrix model does not search for the finest grid, since the scale satisfying the continuum assumption of TFM is found to overlap that of meso-scale structure in a CFB (Wang and Li, 2007). For a specific mesh, EMMS/matrix regards TFM as a filtered or averaged model already, since the averaging over the bi-scale resolution of EMMS/matrix results in the conservation equations of TFM, as shown in Appendix of Wang and Li (2007).

Taking the drag coefficient β_0 derived from Wen and Yu (1966) as the standard, Fig. 1 shows the results of EMMS/matrix in form of a reduced drag coefficient H_D ($H_D = \beta/\beta_0$, heterogeneity index), which is a function of local Reynolds number *Re* and voidage for an air-FCC system. Only the vertical direction of slip velocity is used here for the sake of visualization. Obviously the voidage governs the variation of H_D in most of the range investigated, and the drag force is reduced ($H_D < 1.0$) due to flow heterogeneity. At the two ends of voidage spectrum, which correspond to the packed bed and extremely dilute flow, respectively H_D takes on values near unity, where two-phase "compromise" gives way to either particle dominance or gas dominance. Reynolds number takes the secondary role in reducing drag force except when slip velocity is small. Higher slip velocity generally results in higher values of H_D, in the sense that formation of aggregates is suppressed by higher slip between gas and particles.

EMMS/matrix model aims to solve ten independent variables with seven nonlinear equations and an optimization condition. Mathematically three degrees of freedom implies that the solution space of this nonlinear non-convex programming problem might be 3-D volumes enclosed by curved surfaces. How to discern the physical differences among infinite points in the volumes and to choose the optimal as the final solution remains a mathematical challenge. At the present stage, the algorithm accepts the optimal solution from preassigned nodes, such that the precision of solution depends on the search step or the node number. For Fig. 1, e.g. 1000 nodes were assigned along each coordinate. This is the reason why the surface of Fig. 1 looks smoother than what we have reported in Dong et al. (2008b), where only 100 nodes were used in each direction. Further efforts are needed to seek more exact searching algorithms.

Fig. 2 shows the projected area plot of the above surface in comparison with some curves calculated from literature correlations. Clearly big discrepancies exist on their estimation of the drag coefficient. In general, besides EMMS/matrix, we may distinguish two trends of drag correction within these correlations: the first is represented by the work of Yang et al. (2004), which undergoes a steep drop due to initial clustering and then gradual increase with solid concentration; the second is represented by the correlation of Nieuwland et al. (1994), which decays monotonically with the increase of solids volume fraction. There are also some other contributions need to mention, such as O'Brien and Syamlal (1993), Andrews et al. (2005), which were proposed for specific set of operating conditions and hence hard to compare within this work. With so many choices, one needs to evaluate them prior to use. That is the topic what we will refer to in the following section.

4. Searching for a mesh-independent sub-grid model

If the above drag corrections in Fig. 2 are regarded as results of sub-grid modeling, a critical issue arises concerning self-consistency, that is, which of these drag models are independent of the filter length λ or the mesh size? A mesh-independent sub-grid model allows one to simulate flow with a mesh coarser than the fine grid of direct numerical simulations (DNS). This is exactly what we want to achieve, especially for industrial applications. If

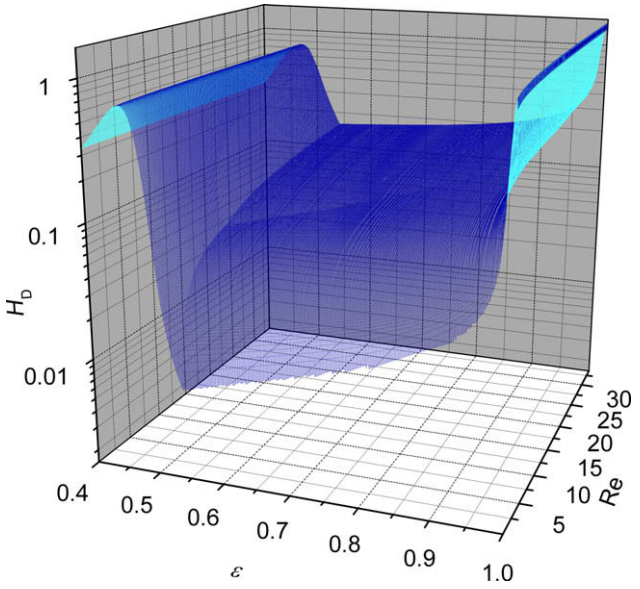

Fig. 1. Surface plot of the heterogeneity index as a function of voidage and Reynolds number ($Re = \varepsilon(u_g - u_p)d_p\rho_g/\mu_g$) for air-FCC particle system ($\rho_g = 1.18\,\mathrm{kg/m^3}$, $\rho_p = 930\,\mathrm{kg/m^3}$, $d_p = 54\,\mu\mathrm{m}$, $U_g = 1.52\,\mathrm{m/s}$, $G_s = 14.3\,\mathrm{kg/(m^2\,s)}$, $\varepsilon_{mf} = 0.4, 3.4 \times 10^{-3} < Re < 34$) (after Lu et al., submitted for publication).

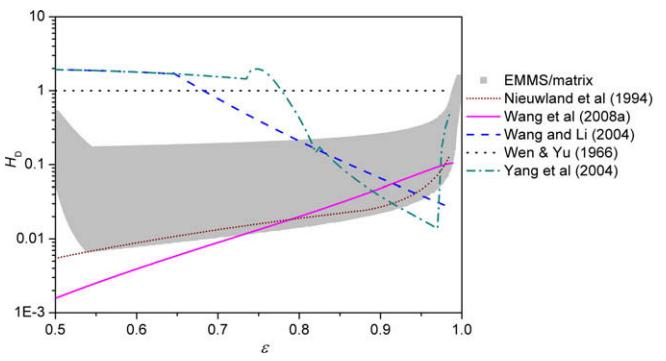

Fig. 2. Projected area plot of the heterogeneity index in Fig. 1 as a function of voidage and its comparison with reported correlations in the literature under the same conditions with those of Fig. 1. (See above-mentioned references for further information.)

there is no range of λ for a sub-grid model where results are λ-independent, however, one has to resort to appropriate DNS solutions.

In order to investigate the grid size effect, we followed the scheme proposed by Agrawal et al. (2001) and restricted our simulation to a periodic 2-D domain of 15×60 mm^2, which is comparable to the coarse grid size commonly used in TFM simulations. The domain was resolved into uniformly spaced, square grids. Fluent® 6.2.16 was used as the solver. The solid stress was closed by the algebraic form of the granular temperature equation derived from the kinetic theory. Fine particles (particle density, $\rho_p = 1500$ kg/m^3; particle diameter, $d_p = 75$ μm) belonging to Geldart group A were uniformly distributed initially with volume fraction of 5%, whose gravity were balanced with the imposed pressure drop in the vertical direction. Periodic boundaries were prescribed in both the lateral and vertical directions, preserving constant solid concentration in the domain. At the beginning of simulations, a small perturbation was introduced in certain grids, followed by the evolution of heterogeneous structure. As no global acceleration exists in a periodic domain, drag force exerted on particles can be related to the effective gravity as follows: $\beta = \varepsilon(1-\varepsilon)(\rho_p - \rho_g)g/u_{slip}$, where ρ_g denotes the gas density, g denotes the gravitational acceleration and u_{slip} denotes the vertical slip velocity. As solids concentration holds constant in the domain, higher slip velocity means lower drag coefficient. More details about computing configuration should be referred to Lu et al. (submitted for publication).

Corresponding to the above section, four typical drag coefficient models were chosen, including EMMS/matrix model (Model M), our previous version of EMMS-based model (Model Y) (Yang et al., 2003, 2004), an EMMS-based model with an improved definition of clusters (Model W) (Wang et al., 2008a) and the hybrid model combining Wen and Yu's and Ergun's relations (Model G) (Gidaspow, 1994). Fig. 3 shows the variation of time-average slip velocity against grid size together with snapshots of the solids distribution. The coordinates are scaled with the terminal velocity of single particles ($u_T \approx 21.84$ cm/s) and particle diameter d_p, respectively. It is interesting to note that the overall appearance of snapshots seems mainly dependent on the mesh resolution. For each model, more elaborate structures are resolved with refining grid. However, the following quantitative comparison reveals their latent difference.

Model G drag coefficient stems from seemingly homogeneous systems, and then it can be viewed as an example irrespective of sub-grid structures. When we gradually increase the grid resolution, the predicted dimensionless slip velocity increases and appears to reach an asymptote at the three smallest grid cases. The nearly doubled slip velocity means that the drag coefficient reduces by 50% during this refining process. The asymptotic slip velocity implies a threshold of scale exists, below which one can reach mesh-independent solution of TFM. This result is similar to the findings of Agrawal et al. (2001). However, whether this

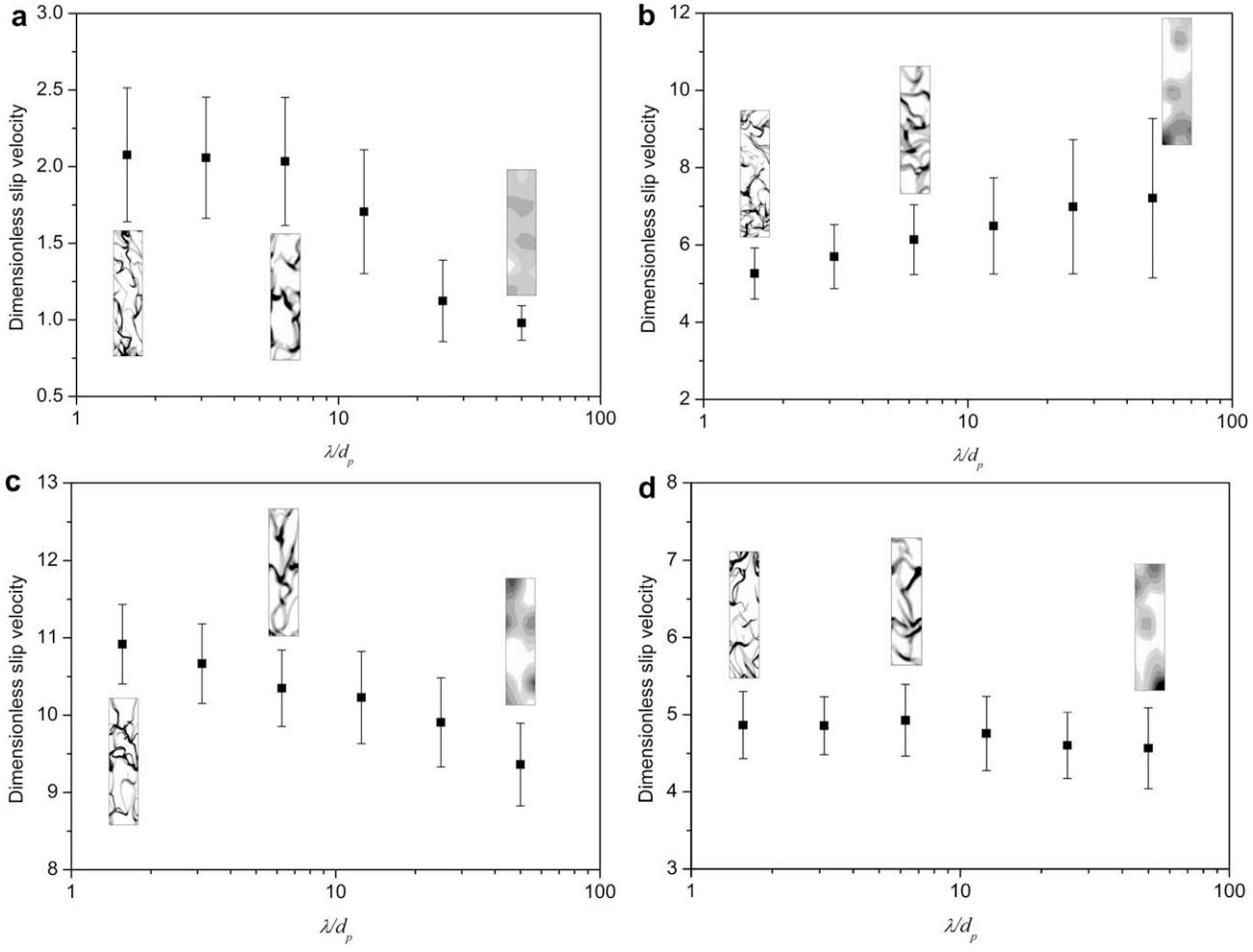

Fig. 3. Effect of grid resolution on time-averaged axial slip velocity scaled with terminal velocity of single particles (u_{slip}/u_T): (a) Model G; (b) Model Y; (c) Model W; (d) Model M. Error bar denotes the square mean root of slip velocity. Physical properties used are akin to air-FCC system ($d_p = 75$ μm, $\rho_p = 1500$ kg/m^3, $\rho_g = 1.3$ kg/m^3, $\mu_g = 1.8 \times 10^{-5}$ Pa s).

mesh-independent solution of TFM really captures the two-phase flow behavior still needs verification from experimental data.

For Models Y and W, their variation of slip velocities are less pronounced than for Model G, showing a decrease of 30% and an increase of 20%, respectively, with refining grid. The predicted slip velocities are larger than that of Model G, and then their drag coefficients are smaller, reflecting the effects of structural factors introduced in these models. However, it seems that no mesh-independent results are obtained over the smallest grid sizes.

By comparison, EMMS/matrix seems to reach its mesh-independent solution all over the range of grid size, in the sense that its predicted slip velocity maintains around five times the terminal velocity. Our explanation for this difference between EMMS/matrix and Models Y and W lies in the fact that the former takes into account both local slip velocity and voidage in formulating the effect of structure, while the latter two take only voidage. As a primary verification, following the method of Reh (1996), we write the local balance equation for a gas–solid flow mixture by regarding the main governing forces acting on particles, viz. drag force, gravity, buoyancy and inertia, then,

$$\frac{3}{4}(1-\varepsilon)\varepsilon^2\frac{\rho_g}{d_p}C_D u_{slip}^2 = (1-\varepsilon)(\rho_p-\rho_g)(g+a). \quad (1)$$

It follows that, in a dimensionless form,

$$\frac{3}{4}Fr\cdot\frac{\rho_g}{\rho_p-\rho_g} = \frac{1}{C_D}\cdot\frac{g+a}{g}, \quad (2)$$

where C_D is the effective drag coefficient for single particles in a cloud of particles, a is the effective inertial term and Fr denotes Froude number ($\mathrm{Fr} = (\varepsilon u_{slip})^2/d_p g$). We can see that, for a given system under force balance, i.e. $a = 0$, the variation of slip velocity depends on voidage, or vice versa. That means the static flow state or structure under the force balance can be determined completely by voidage. This corresponds to the experimental conditions of classical fluidized beds, say, that of Wen and Yu (1966). So it is not surprising that Wen and Yu drag correction for many-body effects can be expressed as $C_D = C_{D0}\cdot\varepsilon^{-4.7}$, where C_{D0} is the standard drag coefficient for a isolated particle. For a given system with inertial effects or accelerations, i.e. $a \neq 0$, slip velocity and voidage can be varied independently. That means the dynamic flow state or structure can be determined only by specifying both voidage and slip velocity. This corresponds to the situation in a CFB. So for CFB simulations, the effective drag correction, or rather, the correction for effective inter-phase momentum exchange, should be determined with both slip velocity and voidage besides physical properties, and this is right the case of EMMS/matrix. We can further expect that more factors could be included for the many-body-effect correction if more forces acting on particles were considered, though they may be of trivial effects for the gas–solid two-phase flow in a CFB.

As mentioned above, Model G converges to its mesh-independent solution, though it is different from EMMS/matrix solution. Then, which solution is closer to the real behavior? In what follows we will try to give our answer by evaluating the results of fine-grid simulation and EMMS/matrix sub-grid simulation of a CFB riser.

Fig. 4 shows a series of predicted axial profiles of voidage of a CFB riser by using different drag correlations with different grid resolutions. This riser has an inner diameter of 9 cm and a height of about 10.5 m, and more of its configuration has been detailed in the literature (Li and Kwauk, 1994; Yang et al., 2004; Wang and Li, 2007). The simulation adopts a circulating mode by specifying the gas velocity at the bottom inlet and the initial solids inventory, leaving free the solids flux by recirculating solids out of the outlet into the sidewall inlets. In general, Model G overestimates the inter-phase momentum transfer in the riser, and hence predicts a much uniform distribution of solids across the riser. Grid refining affects little on the axial profiles, as the uniform distribution has no degree of freedom for variation under a constant solids inventory. The large discrepancy was ameliorated greatly by using Model Y, by which a dilute top coexisting with a dense bottom was reproduced. For this test case, the best agreement with experimental data was achieved when using EMMS/matrix. As for predicted solids flux, the asymptotic result of Model G is around 170 kg/m^2 s, about 10 times the experimental data of 14.3 kg/m^2 s, while the best result is obtained again with EMMS/matrix, which is around 19 kg/m^2 s. The same tendency can be found when we simulate the above riser using non-circulating mode and simulate the riser of Horio et al. (1988), details of which should be referred to Lu et al. (submitted for publication).

One may question why the conventional drag model fails even if the clusters are resolved with fine grid. The probable reason lies in

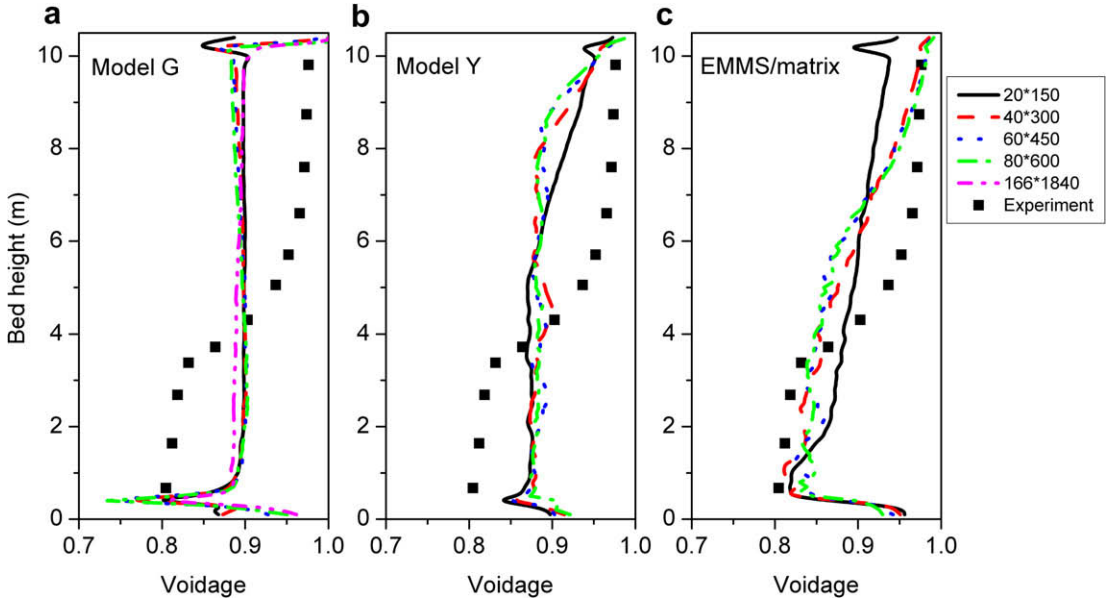

Fig. 4. Effect of grid resolution on the time-averaged axial profiles of voidage: (a) Model G; (b) Model Y and (c) EMMS/matrix. (Air-FCC particle system from Li and Kwauk (1994), $\rho_p = 930$ kg/m^3, $d_p = 54$ μm, $U_g = 1.52$ m/s, initial bed height 1.855 m, initial packing voidage 0.4.)

the fact that the two-phase flow is different from the single-phase flow in nature. The sub-grid contribution for single-phase flow goes to zero as one reaches the Kolmogorov scale, because the Navier–Stokes (NS) equation still holds true on the Kolmogorov scale in the sense that clear-cut scale separation exists between the molecular movement and the continuum description of NS equations. For the two-phase flow, however, the widely cited two-fluid model (TFM) cannot bear the same role as the NS equations do for single-phase flow, in the sense that no scale separation exists between the macroscopic granular movement and pseudo-fluid assumption of TFM, as discussed in Wang and Li (2007). The sub-grid contribution for two-phase flow hence does not vanish even though TFM with conventional drag models reaches its asymptotic solution along with grid refining. EMMS/matrix model has basically different governing equations from those of TFM in that its conservation equations are doubled in terms of dense phase and dilute phase. As discussed in Wang et al. (2007, 2008b) and summarized in the following section for the flow regime transition, EMMS-based models, in their own right, allow bifurcation or coexistence of two solutions for one given conditions. The intrinsically sub-grid contribution of structures can hence be captured.

It is interesting to note that grid refining has some influence on the predicted profiles of EMMS/matrix in the riser though its influence, as shown in Fig. 3, is trivial in the periodic domain. The probable reason is that the current version of EMMS/matrix only takes into account the effects of structure on the drag force, while the other factors of importance but not regarded in the current comparison, say, solid stress, may vary with grid refining. Further efforts are needed to elucidate this issue.

Based on the above comparisons, two remarks can be drawn at least for the test cases in this article: first, TFM without sub-grid drag models cannot reproduce quantitatively the meso-scale structure, and hence fails to capture the flow behavior in a CFB riser, though grid refining process do helps reach its asymptote; second, EMMS/matrix seems to reach a mesh-independent solution of the structural effect at the sub-grid level, though more verification are necessary to validate its applicability under different conditions. More efforts should also be undertaken to account for the effects of structure on some other factors such as the solid stress.

5. Flow regime transition and operating diagram

To delineate the choking and related flow regime transitions and to validate our EMMS-based models, both EMMS model in itself and CFD coupling EMMS/matrix have been used to simulate the states of flow over a wide range of operating conditions (Wang et al., 2007, 2008b). As shown in Fig. 5a, the apparent flow regime diagrams can be illustrated with a set of iso-aeration describing the relation between solid flux G_s and averaged solids fraction of the riser ε_{s0} at specified superficial gas velocity U_g. The typical diagram embraces at least three regimes, i.e. dilute transport to the left of the diagram, dense upflow to the right, and in between the jump transition in shaded area. A continuous transition can also be defined above the critical point or the summit of the shaded area. The jump transition area is marked by the coexistence of both the dense upflow and the dilute transport, over which the iso-aeration levels off with saturation carrying of particles. Such a jump change can be related with the widely cited "choking" phenomena in both pneumatic transport and circulating fluidized beds (Wang et al., 2008b). As reviewed by Bi et al. (1993) and Yang (2004), choking usually occurs with a rapid increase of pressure drop, when the solids flux is kept constant with decrease of the conveying gas velocity. In the following discussion, the term "choking" is coined to restrict its meaning to the hydrodynamic jump change addressed above and also detailed elsewhere (Wang et al., 2007). More phenomena related with geometric or instrumental limitations are left untouched here.

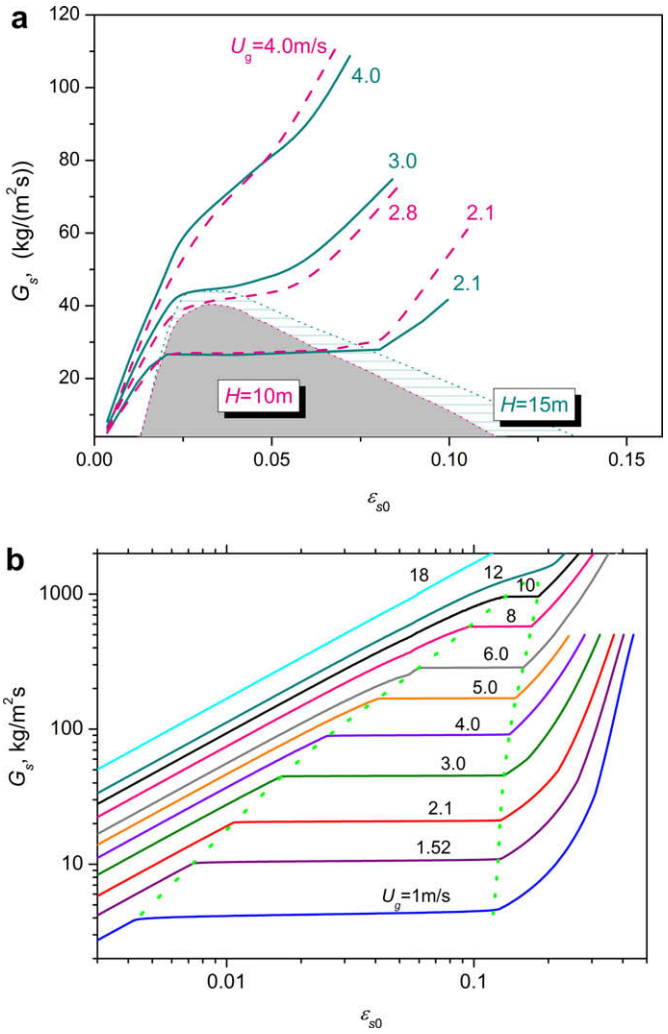

Fig. 5. Apparent and intrinsic flow regime diagrams calculated for the air-FCC system (fluid catalytic cracking particle, $d_p = 54$ μm, $\rho_p = 930$ kg/m^3) (after Wang et al., 2008). (a) Apparent flow regime diagrams for 10 m and 15 m high risers, bell-shaped areas referring to related choking area, respectively, and (b) intrinsic flow regime diagram without limitation of riser height.

Quantitative comparison on flow regime transitions has also been reported (Wang et al., 2007; Li et al., 2007). However, as illustrated by the expanded choking area in Fig. 5a for a 15 m high riser, the flow regimes are also affected by factors such as the riser height and inlet/outlet configurations. In our opinion, this is at least one of the major reasons that cause disputes in understanding the choking. However, the geometrical limitation always exists and differs for specific configurations in CFD simulation. To delineate the intrinsic hydrodynamic aspects, we further resort to the original EMMS model to describe the state of motion of fluidized beds (Wang et al., 2008b).

Fig. 5b gives the intrinsic flow regime diagram calculated with the original EMMS model for the air-FCC system. Similar flow regime partitions can be distinguished over the range of G_s and ε_{s0}, except that the choking area is much larger but somewhat askew. Compared to the apparent diagram in Fig. 5a, we can conclude that the extent of the choking area varies, with the riser height in appearance, and expands, as illustrated in Fig. 6, due to increased capacity of higher column for holding solids. The critical point, in turn, will rise to a higher position as to the critical gas velocity U_g^* and the critical solids flux G_s^*. Thus, the choking observed in a higher riser may be absent for a short riser, as it may be easily ob-

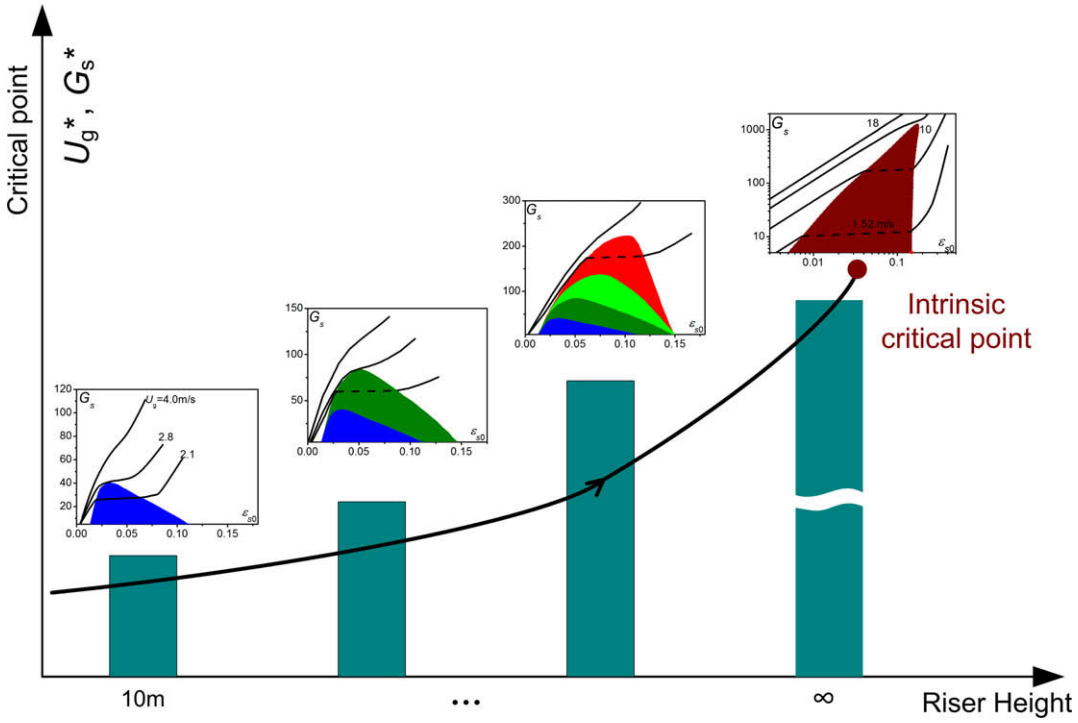

Fig. 6. Riser height decides the variation from apparent to intrinsic flow regime diagrams. Dark cyan columns represent different riser heights with relevant flow regime diagram sketched above, and the curve denotes the variation of the critical point with the final end of intrinsic critical point.

scured by the comparatively strong effects of the developing flow near the inlet/outlet. In general, the intrinsic flow regime is important to understand the real hydrodynamic aspects behind various appearances. On the basis of it, we can expect to draw a series of the operating diagram, which demands geometrical parameters besides commonly believed parameters such as gas velocity and solids flux, and thus to help CFB operation.

6. Multiscale modeling of mass/heat transfer

Inhomogeneous distribution of particles may promote bypass of gas around clusters, and thus, decrease the effective interphase mass/heat transfer rate. To resolve this influence of the structure, the bi-scale resolution of EMMS is followed by our newly proposed multiscale mass transfer model EMMS/mass (Dong et al., 2008a,b). The current version of EMMS/mass accepts the structure parameters from EMMS/matrix and puts them to account for the heterogeneous mass transfer within a grid. Obviously, it also allows the other closure relations to substitute these structure parameters. The mass conservation equations of EMMS/mass are presented for the gas mixture and components in the dense phase and the dilute phase, respectively. Take for example the vaporization of component A, the equations read

$$\frac{\partial}{\partial t}(\phi_k \varepsilon_k \rho_g) + \nabla \cdot (\phi_k \varepsilon_k \rho_g \mathbf{u}_{gk}) - S_k - \Gamma_{ik} = 0, \tag{3}$$

$$\frac{\partial}{\partial t}(\phi_k \varepsilon_k \rho_g x_{A,k}) + \nabla \cdot (\phi_k \varepsilon_k \rho_g x_{A,k} \mathbf{u}_{gk} - \phi_k \varepsilon_k \rho_g D_m \nabla x_{A,k}) - S_k - \Gamma_{A,ik} = 0, \tag{4}$$

where the volume fraction ϕ_k are f and $(1-f)$ for the dense phase and dilute phase, respectively, $x_{A,k}$ denotes the mass fraction of A in the phase k, D_m denotes the molecular diffusion coefficient, Γ_{ik} denotes the mass exchange rate between the dense and dilute phases, and the vaporization source term S_k reads

$$S_k = \phi_k k_k (1-\varepsilon_k) \alpha_p \rho_g (x_{A,sat} - x_{A,k}), \tag{5}$$

where k_k denotes the mass transfer coefficient between gas and particles in homogeneous suspension of phase k. The meso-scale mass exchange rate of A, $\Gamma_{A,ik}$, mainly depending on the cluster renewal or breakup, can be approximated by $\Gamma_{ik} x_{A,j}$ if it is dominated by convection, where subscript j denotes the carrier gas. That is, if Γ_{ik} is from the phase "c" to "f", then $x_{A,j} = x_{A,c}$, else, $x_{A,j} = x_{A,f}$.

For an overall evaluation of the mass transfer, one can take parameters $(\phi_k, \varepsilon_k, u_{gk})$ from the original EMMS model. For example, in a one-dimensional, steady and fully developed riser, clusters were assumed invariant, then Eqs. (3)–(5) were simplified in that all terms related with $\partial/\partial t, \partial/\partial \mathbf{r}$ except $\partial/\partial z$ were ignored (Dong et al., 2008a). With the structure parameters from EMMS, the solution of Eqs. (3)–(5) was plotted in Fig. 7(a) in terms of the overall Sherwood number Sh_{ovr} as a function of superficial Reynolds number $Re_0 (= U_g d_p \rho_g / \mu_g)$ and ε. The coordinate ranges of Re_0 and ε were obtained by varying U_g (1–21 m/s) and G_s (10–170 kg/m^2 s). An obvious jump change of Sh_{ovr} can be found around 50–100 of Re_0, which reflects the jump change effect of voidage encountered at choking. Experimental data of Wang (2002) and Subbarao and Gambhir (2002), both having Schmidt number $Sc \approx 2.5$ with naphthalene and air, were plotted against model prediction. The comparison shows good agreement between model and data.

Fig. 7(b) is a projection of Fig. 7(a) over the plane of Sh_{ovr} against Re_0. The magenta circles together with shaded area denote the model results. It is evident that Sh_{ovr} is a multi-valued function of Re_0, that is, Re_0 is insufficient for correlating Sh_{ovr} in a CFB. This is the reason why the conventional correlations of mass-transfer coefficient scattered by several orders of magnitudes. The jump change around 50–100 of Re_0 owing to the choking is more distinct on this plane. It is interesting to note that the curves of Sherwood number for classical fluidized beds and fixed beds also display a similarly abrupt change around the same range of Re_0 (Kunii and Levenspiel, 1991). One may expect, accordingly, that certain jump

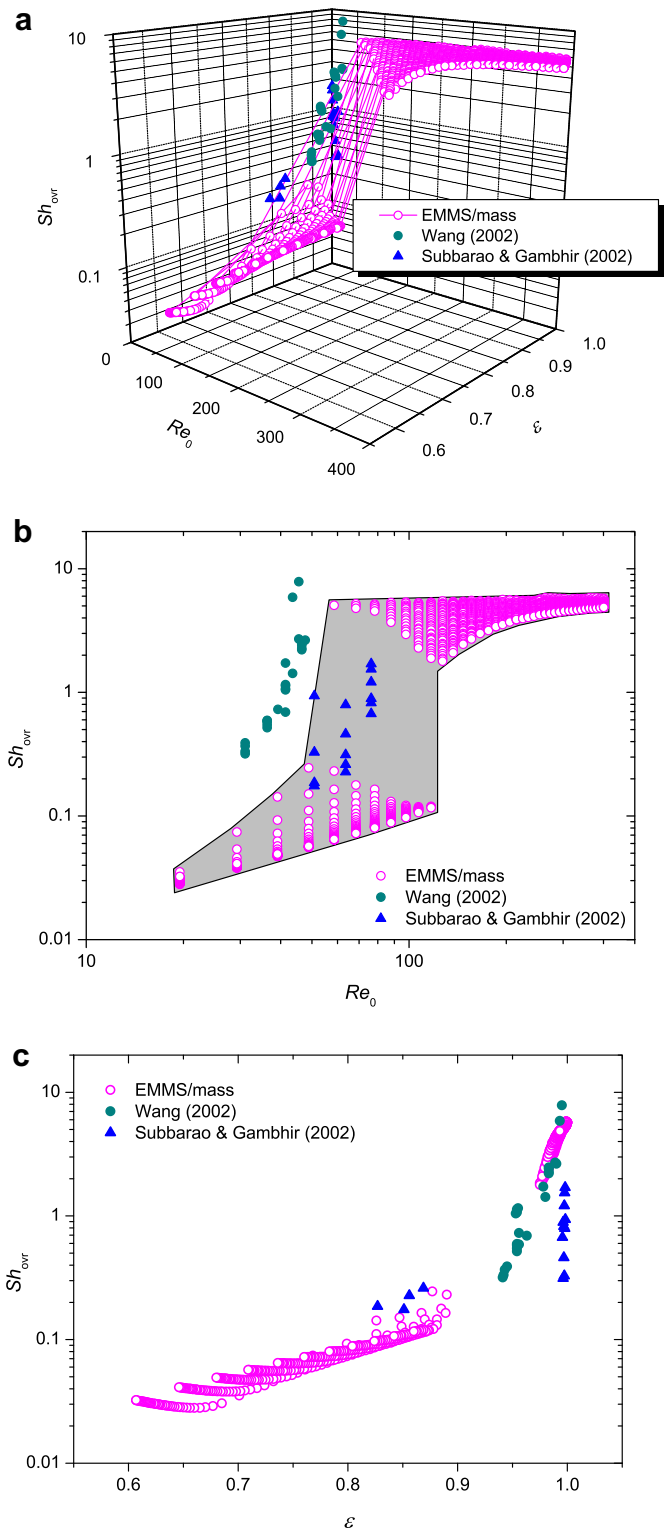

Fig. 7. Comparison of overall Sherwood number Sh_{ovr} between this work and the literature data. (a) Surface dots of EMMS/mass-calculated Sh_{ovr} as a function of Re_0 and ε; (b) dots of EMMS/mass-calculated Sh_{ovr} as a function of Re_0 and (c) dots of EMMS/mass-calculated Sh_{ovr} as a function of ε. Dark cyan solid dots refers to data of Wang (2002) (sublimation of naphthalene into air, $\rho_p = 1162\ kg/m^3$, $d_p = 300\ \mu m$, dilution ratio is 1/9), where experimental voidage is averaged over the whole riser; blue triangle refers to data of Subbarao and Gambhir (2002) (adsorption of naphthalene in air over sand, $\rho_p = 2600\ kg/m^3$, $d_p = 196\ \mu m$), where voidage is calculated with EMMS (http://pevrc.ipe.ac.cn/emms/emmsmodel.php3) (Ge and Li, 2002), as no voidage data is reported in the literature.

change of state of motion occurs in classical fluidized beds, as is the choking in circulating fluidized beds. It seems possible to unify the understanding on mass transfer in both classical- and circulating-fluidized beds by extending our current framework.

The dispersed data in Fig. 7(b) can be attributed to the neglect of voidage. As shown in Fig. 7(c), except for a little scatter over the range of dense flow, Sh_{ovr} correlates well with ε. It seems that voidage is the most important factor to determine the mass transfer in a CFB, at least for this simplified test case. One should note, however, that the profile of Sh_{ovr} is quite steep when the voidage approaches unity and it even manifests a multi-valued dependency on the voidage. That means Reynolds number is important when the gas velocity is high and the two-phase suspension is dilute. It should also be noted, as shown in Fig. 7(b), that current mass transfer experiments for a CFB were usually limited to a narrow range of Re_0 and the experimental values of voidage were even unreported. We still need experimental efforts to investigate Sh_{ovr} over wider ranges of factors to better understand the complex mass transfer.

For detailed evaluation of the mass transfer in a riser, one can take parameters $(\phi_k, \varepsilon_k, u_{gk})$ from EMMS/matrix model in CFD simulations (Dong et al., 2008b). Fig. 8 shows typical results through simulating an ozone decomposition experiment (Ouyang et al., 1995). It is demonstrated that the conventional approach without considering the structural effects gives poor results in that the relevant mass transfer rate and ozone decomposition rate are overestimated significantly (Fig. 8c). Considering the effect of structures on hydrodynamics improves results to a great extent, but discrepancy still exists (Fig. 8b). The best prediction is obtained only when the structural effects on both flow and mass transfer are considered by using EMMS/matrix and EMMS/mass, respectively (Fig. 8a). This comparison validates the importance of multiscale mass transfer modeling for a CFB reactor.

7. Emerging virtual experimentation of CFB

At present, most of CFD simulations of CFB are still confined to simplified 2-D risers, thus neglecting the hybrid influence of the other sections of the whole loop. To investigate CFB as an integrated system, recently we performed a 3-D, real-size and full-loop, time-dependent simulation of a semi-industry CFB (8.5 m in height, 0.411 m in riser diameter), which was established by the group of Prof. Reh (Herbert et al., 1999; Zhang et al., 2008). Fig. 9 shows a characteristic snapshot of the solid distribution, together with two iso-surface plots of solid volume fraction of 2% and 29%, respectively. The time-average profile of the solid volume fraction is also given against experimental data. It is clear from sectioned iso-surfaces in Fig. 9b and c that dense clusters mainly flow downward against bypassing gas near the wall, while dilute suspensions of particles tend to be entrained by neighboring gas flow in the center. The magnitude of upward velocity of solids is generally higher than the downward velocity in dense clusters, reflecting the acceleration effects of gas entraining. Quantitative comparison between simulation and experimental data in Fig. 9(d) shows good agreement.

This is just a primary attempt to the 3-D, full-loop, time-dependent investigation of CFB behavior through the multiscale simulation. On the basis of it, one can expect to probe certain complex phenomena concerning the interrelation around the whole loop, e.g. choking and flow regime transitions, and to clarify the underlying mechanisms that cause disputes. Further with reaction kinetics added, we expect an emerging paradigm that the multiscale CFD simulation helps provide comprehensive details of a CFB and then plays critical role in troubleshooting and scale-up of industrial units.

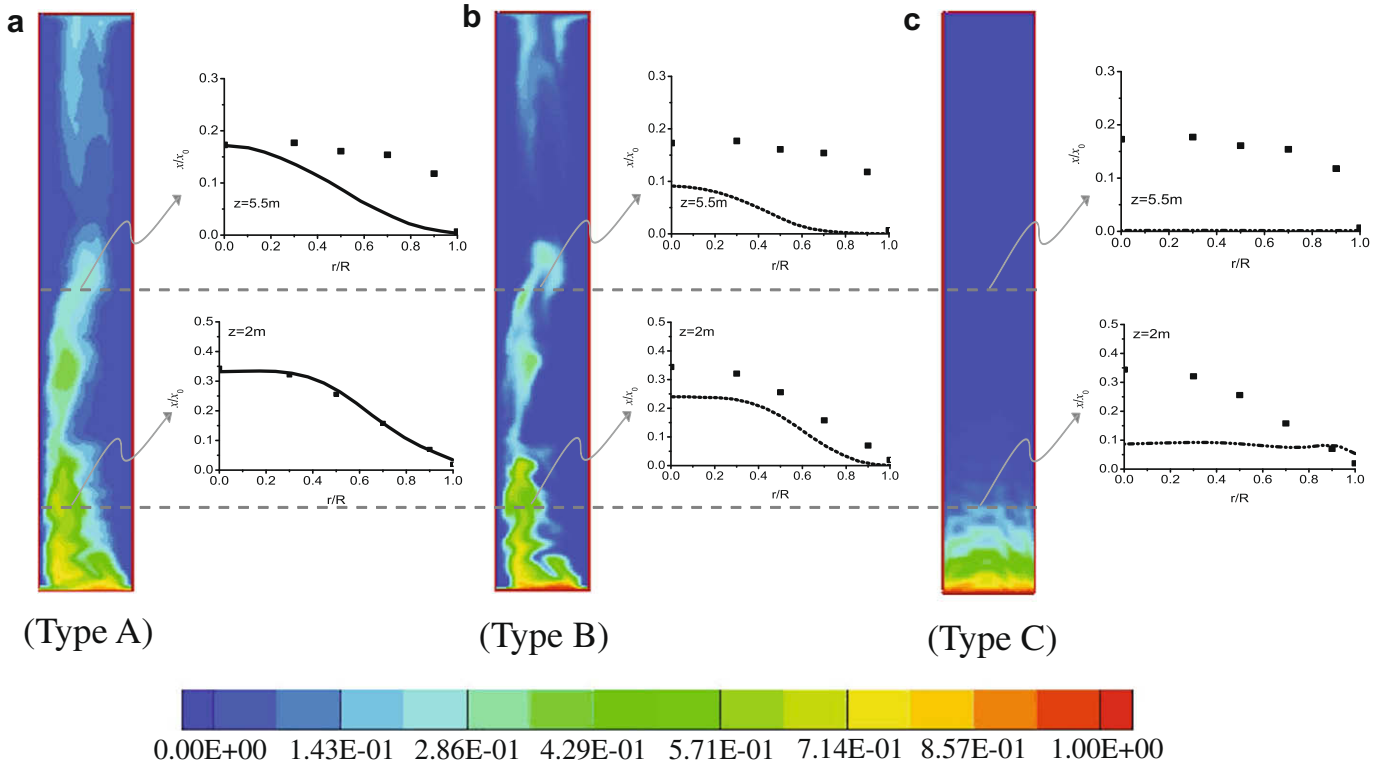

Fig. 8. Snapshots of dimensionless ozone concentration and related time-averaged radial profiles at different heights (experiment: Ouyang et al. (1995); $U_g = 3.8$ m/s, $G_s = 106$ kg/m^2 s, $k_r = 57.21$ (m^3/(m^3 s) (catalysts)). (a) EMMS/matrix for flow and EMMS/mass for mass transfer; (b) only flow structure is considered through EMMS/matrix drag coefficient, mass transfer model is the conventional and (c) conventional CFD model for both flow and mass transfer without structural consideration. (Color spectrum is in log scale.) (After Dong et al., 2008b.)

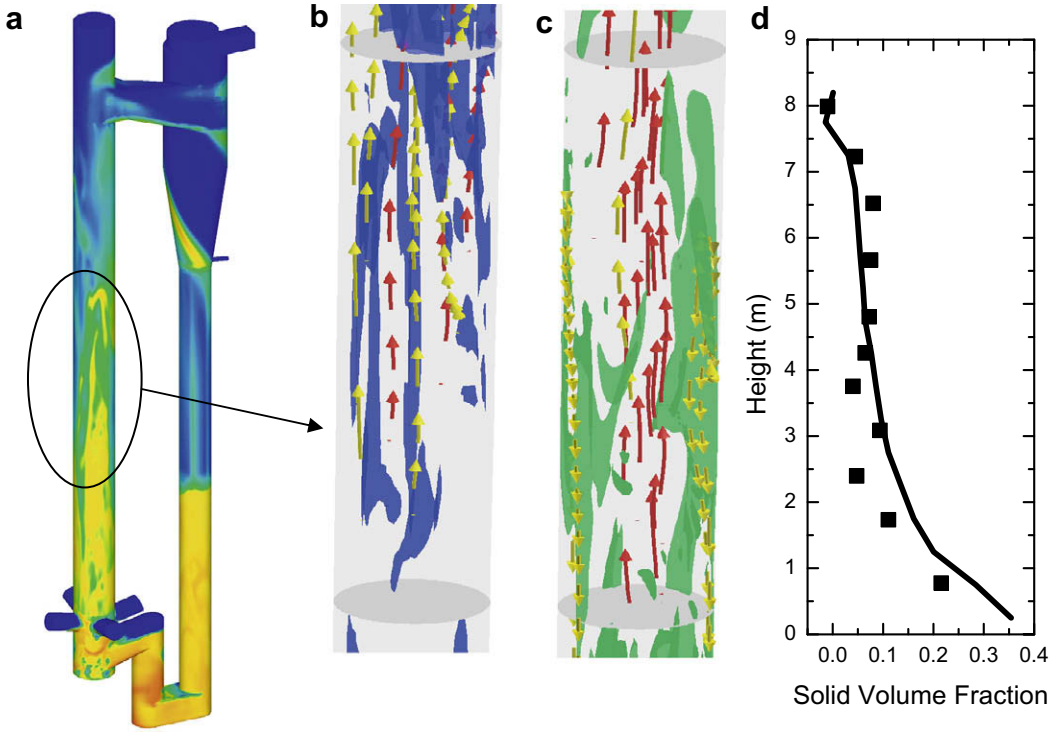

Fig. 9. Snapshots of solid volume fraction distribution and time-average profile of solid volume fraction against data. (a) A snapshot of solid volume fraction distribution; (b) iso-surface plot of solid volume fraction of 0.019 between $z = 3.66$ and 5.8 m; (c) iso-surface plot of solid volume fraction of 0.29 between $z = 3.66$ and 5.8 m and (d) solid squares denotes data and solid line represents simulation results. In (b) and (c), red arrows represent gas streamlines, yellow arrows represent solid streamlines. (Air-Fcc particle system, $\rho_p = 1400$ kg/m^3, $d_p = 60$ μm, $U_g = 3.5$ m/s, solids inventory $I = 277.7$ kg.) (After Zhang et al., 2008.) (For interpretation of color mentioned in this figure legend the reader is referred to the web version of the article.)

8. Concluding remarks and prospects

Meso-scale structure is of critical importance to CFB applications. The multiscale CFD can help grasp the meso-scale structure. TFM with conventional drag model has its mesh-independent solution in terms of reaching the asymptote in periodic domains. However, this mesh-independent solution is inexact in the sense that it overestimates the drag coefficient and fails to capture the S-shaped axial profile of voidage in CFB risers. By comparison, EMMS/matrix model seems to reach a mesh-independent solution of the effect of meso-scale structure, and succeeds in predicting the axial profiles of voidage and further the flow regime transitions. In practice, the apparent flow regimes are affected by geometric factors besides hydrodynamics. This is one of the major reasons that cause disputes in understanding the choking and related transitions. As to mass transfer, Reynolds number is insufficient for correlating the overall Sherwood number in a CFB. This is the main reason why the conventional correlations of Sherwood number scatter by several orders of magnitudes. The jump change of state of motion around 50–100 of Reynolds number can be expected to unify the understanding on the abrupt decay of Sherwood number in both classical- and circulating-fluidized beds. Finally, on the basis of reliable models, one can expect that the 3-D, full-loop, time-dependent, multiscale simulation can help discern, trouble-shoot and even scale up CFB reactors. We are facing an emerging paradigm of virtual experiment of CFBs.

Acknowledgements

This work is financially supported by the National Natural Science Foundation of China under Grant Nos. 20490201, 20221603, 20606033 and by the MOST under Grant Nos. 2007AA050302-03 and 2006AA030201.

References

Agrawal, K., Loezos, P.N., Syamlal, M., Sundaresan, S., 2001. The role of meso-scale structures in rapid gas–solid flows. J. Fluid Mech. 445, 151–185.

Andrews, A.T., Loezos, P.N., Sundaresan, S., 2005. Coarse-grid simulation of gas–particle flows in vertical risers. Ind. Eng. Chem. Res. 44, 6022–6037.

Bi, H.T., Grace, J.R., Zhu, J.-X., 1993. Types of choking in vertical pneumatic systems. Int. J. Multiphase Flow 19, 1077–1092.

Breault, R.W., 2006. A review of gas–solid dispersion and mass transfer coefficient correlations in circulating fluidized beds. Powder Technol. 163, 9–17.

Chen, J.C., 2003. Heat transfer. In: Yang, W.C. (Ed.), Handbook of Fluidization and Fluid–Particle Systems. Marcel Dekker Inc., New York.

Ding, J., Gidaspow, D., 1990. A bubbling fluidization model using kinetic theory of granular flow. AIChE J. 36, 523–538.

Dong, W., Wang, W., Li, J., 2008a. A multiscale mass transfer model for gas–solid riser flows: part 1 — sub-grid model and simplification. Chem. Eng. Sci. 63, 2798–2810.

Dong, W., Wang, W., Li, J., 2008b. A multiscale mass transfer model for gas–solid riser flows: part 2 — sub-grid simulation of ozone decomposition. Chem. Eng. Sci. 63, 2811–2823.

Ge, W., Li, J., 2002. Physical mapping of fluidization regimes — the EMMS approach. Chem. Eng. Sci. 57, 3993–4004.

Gidaspow, D., 1994. Multiphase Flow and Fluidization: Continuum and Kinetic Theory Descriptions. Academic Press, Boston.

Gidaspow, D., Jung, J., Singh, R.K., 2004. Hydrodynamics of fluidization using kinetic theory: an emerging paradigm 2002 Flour–Daniel lecture. Powder Technol. 148, 123–141.

Grace, J.R., Issangya, A.S., Bai, D., Bi, H.T., Zhu, J., 1999. Situating the high-density circulating fluidized bed. AIChE J. 45, 2108–2116.

Herbert, P., Reh, L., Nicolai, R., 1999. The ETH experience: experimental database and results from the past eight years. AIChE Symp. Ser. 321, 61–66.

Horio, M., Morishita, K., Tachibana, O., Murata, N., 1988. Solid distribution and movement in circulating fluidized beds. In: Basu, P., Large, J.F. (Eds.), Circulating Fluidized Bed Technology II. Pergamon Press, Oxford, pp. 147–154.

Igci, Y., Andrews, A.T., Sundaresan, S., Pannala, S., O'Brien, T., 2008. Filtered two-fluid models for fluidized gas–particle suspensions. AIChE J. 54, 1431–1448.

Kunii, D., Levenspiel, O., 1991. Fluidization Engineering, second ed. Butterworth-Heinemann, Boston.

Kwauk, M., 1994. Fast fluidization. Advances in Chemical Engineering, vol. 20. Academic Press, New York.

Li, Y., 1994. Hydrodynamics. In: Kwauk, M. (Ed.), Advances in Chemical Engineering, vol. 20. Academic Press, New York, pp. 85–146.

Li, J., Kwauk, M., 1994. Particle–Fluid Two-Phase Flow: The Energy-Minimization Multi-Scale Method. Metallurgy Industry Press, Beijing.

Li, J., Kwauk, M., 2001. Multiscale nature of complex fluid–particle systems. Ind. Eng. Chem. Res. 40, 4227–4237.

Li, J., Kwauk, M., 2003. Exploring complex systems in chemical engineering — the multi-scale methodology. Chem. Eng. Sci. 58, 521–535.

Li, J., Ge, W., Zhang, J., Gao, S., Wang, W., Yang, N., Sun, Q., Gao, J., 2007. Analytical multi-scale methodology for fluidization systems — retrospect and prospect. In: Bi, X., Berruti, F., Pugsley, T. (Eds.), Fluidization XII. Engineering Conference International, New York, pp. 15–30.

Lu, B., Wang, W., Li, J., 2008. Searching for a mesh-independent sub-grid model for gas–solids riser flows. Chemical Engineering Science, submitted for publication.

Neri, A., Gidaspow, D., 2000. Riser hydrodynamics: simulation using kinetic theory. AIChE J. 46, 52–67.

Nieuwland, J.J., Huizenga, P., Kuipers, J.A.M., Van Swaaij, W.P.M., 1994. Hydrodynamic modeling of circulating fluidized beds. Chem. Eng. Sci. 49, 5803–5811.

O'Brien, T.J., Syamlal, M., 1993. Particle cluster effects in the numerical simulation of a circulating fluidized bed. In: Avidan, A.A. (Ed.). Circulating Fluidized Bed Technology IV, New York, pp. 345–350.

Ouyang, S., Li, X.-G., Potter, O.E., 1995. Circulating fluidized bed as a catalytic reactor: experimental study. AIChE J. 41, 1534–1542.

Reh, L., 1996. Fluid dynamics of CFB combustors. In: Kwauk, M., Li, J. (Eds.), Circulating Fluidized Bed Technology V. Science Press, Beijing, pp. 1–15.

Soundararajan, S., Dalai, A.K., Berruti, F., 2001. Modeling of methanol to olefins (MTO) process in a circulating fluidized bed reactor. Fuel 80, 1187–1197.

Subbarao, D., Gambhir, S., 2002. Gas to particle mass transfer in risers. In: Proceedings of 7th International Circulating Fluidized Beds Conference, Canadian Society for Chemical Engineering, Niagara Falls, pp. 97–104.

Sundaresan, S., 2006. Analysis of the flow in inhomogeneous particle beds using the spatially averaged two-fluid equations. Int. J. Multiphase Flow 32, 106–131.

Wang, L., 2002. Multi-scale mass transfer model and experimental validation for heterogeneous gas–solid two-phase flow. Doctor dissertation, Chinese Academy of Science, Beijing.

Wang, W., Li, Y., 2004. Simulation of the clustering phenomenon in a fast fluidized bed: the importance of drag correlation. Chin. J. Chem. Eng. 12, 335–441.

Wang, W., Li, J., 2007. Simulation of gas–solid two-phase flow by a multiscale CFD approach — extension of EMMS to sub-grid level. Chem. Eng. Sci. 62, 208–231.

Wang, W., Lu, B., Li, J., 2007. Choking and flow regime transitions: simulation by a multi-scale CFD approach. Chem. Eng. Sci. 62, 814–819.

Wang, J., Ge, W., Li, J., 2008a. Eulerian simulation of heterogeneous gas–solid flows in CFB risers: EMMS-based sub-grid scale model with a revised cluster description. Chem. Eng. Sci. 63, 1553–1571.

Wang, W., Lu, B., Dong, W., Li, J., 2008b. Multiscale CFD simulation of operating diagram for gas–solid risers. Can. J. Chem. Eng. 86, 448–457.

Wen, C.Y., Yu, Y.H., 1966. Mechanics of fluidization. Chem. Eng. Symp. Ser. 62, 100–111.

Yang, W.C., 2004. Choking revisited. Ind. Eng. Chem. Res. 43, 5496–5506.

Yang, N., Wang, W., Ge, W., Li, J., 2003. Choosing structure-dependent drag coefficient in modeling gas–solid two-phase flow. Chin. Particuol. 1, 38–41.

Yang, N., Wang, W., Ge, W., Li, J., 2004. Simulation of heterogeneous structure in a circulating fluidized-bed riser by combining the two-fluid model with the EMMS approach. Ind. Eng. Chem. Res. 43, 5548–5561.

Zhang, J., Ge, W., Li, J., 2005. Simulation of heterogeneous structures and analysis of energy consumption in particle–fluid systems with pseudo-particle modeling. Chem. Eng. Sci. 60, 3091–3099.

Zhang, N., Lu, B., Wang, W., Li, J., 2008. Virtual experimentation through 3-D full-loop CFD simulation of a CFB. Particuology 6, 529–539.